Theory of luminescence spectra from δ-doping structures: Application to GaAs

G. M. Sipahi, R. Enderlein, L. M. R. Scolfaro, J. R. Leite, E. C. F. da Silva, and A. Levine
Instituto de Física da Universidade de São Paulo, Caixa Postal 66318, 05315-970 São Paulo, SP, Brazil
(Received 29 July 1997)

A general procedure for calculating luminescence spectra from δ-doping structures of semiconductors is developed. The electron and hole states are self-consistently calculated within the eight-band Kane model. Explicit results are obtained for p-type δ-doping wells and superlattices in GaAs. For a prototype superlattice (SL) it is demonstrated how the luminescence spectra of δ-doping structures depend on their self-consistent potentials, band structures, and oscillator strengths of radiative recombination processes between extended electron and confined hole states. Wave-vector conserving (direct) and nonconserving (indirect) transitions are considered. Luminescence spectra are calculated for a series of p-type δ-doping SL's, varying their sheet doping concentrations, doping spreads, and periods. A comparison with experimental spectra shows that direct transitions may be ruled out. The indirect spectra are dominated by an emission band below the gap whose structures reflect the various occupied hole subbands. Increasing the temperature, the calculated hole emission bands become stronger, in contrast with experiment. This discrepancy is solved by means of a photoinduced electron confinement. [S0163-1829(98)05104-2]

I. INTRODUCTION

δ doping in GaAs and other materials is now widely used in semiconductor basic research and device applications.[1,2] A unique feature of this particular type of doping is that it gives rise to qualitatively different localized carrier states as compared to those in homogeneously doped semiconductors. Provided the sheet dopant concentration is high enough, the common localized impurity states within the fundamental gap disappear, and instead confined states occur having energies within the former bulk bands.[3–16] This happens because an ionized dopant layer creates a one-dimensional quantum well perpendicular to the layer in which the released carriers are confined. Within the layer, the carriers are free to move, thus the confined levels are widened into subbands. As there are no empty states in the gap, the majority carriers must populate the lowest subband states and form a two-dimensional carrier gas.

The above model of the electronic structure of δ-doped semiconductors has been confirmed by photoluminescence (PL) measurements in GaAs (Refs. 12,17–21) and Si.[22] In PL, the photoexcited minority carriers radiatively recombine with the quasi-two-dimensional (Q2D) majority carriers of the δ-doping wells. Since the minority carriers are in extended states and have energies close to the respective bulk band bottoms, their radiative recombination should result in luminescence peaks below the gap, each peak corresponding to a certain majority carrier subband. Experimentally, such Q2D emission peaks have been observed in p-type δ-doping structures in GaAs (Refs. 12,18–21) and Si.[22] Surprisingly, the PL spectra from n-type δ-doping structures in GaAs are qualitatively different from those for p-type structures in this material. In the n-type case, a relatively strong emission is observed above the gap,[17] while the Q2D emission band below the gap is rather weak or even not observable at all. To make it visible, the n-type wells were placed close to the surface or to a (Al,Ga)As barrier,[17] confining the minority holes in this way and enhancing the oscillator strength of their radiative recombination with the confined electrons. But even then no clear evidence of a Q2D electron emission has been obtained. An explanation for the different PL spectra from n-type and p-type δ-doping structures has been given in Ref. 23. In both types of structures the radiative recombination probability is proportional to the overlap integrals between majority and minority carrier envelope functions. The potential region, which represents a well for the majority carriers, is seen as a barrier from the point of view of the minority carriers. The latter must tunnel through this region in order to overlap with the majority carriers being localized there. This causes the overlap integrals to be smaller if the barriers for the minority carriers are higher. Exactly this is what happens for n-type structures. Because the electrons are not as well localized at the ionized dopant sheet as the heavy holes are, they screen the Coulomb potential of this sheet less effectively than the holes do. Thus, the electron wells of n-type structures come out several times deeper than the hole wells for p-type structures. This reduces the PL intensities of the former structures with respect to the latter, owing to well depth dependence of the overlap integrals.[23]

Because of the difficulties of observing PL peaks originating from the confined majority carrier gas of n-type δ-doping structures, PL measurements on δ-doping systems have almost exclusively been devoted to p-type structures where the PL signals from the confined majority carrier gas are strong enough to be detected even without confining the minority carriers between barriers. The experimental line shapes of the Q2D emission bands may be understood by means of similar tunneling arguments as the ones used above, employing in addition the different tunneling probabilities for heavy and light holes into the hole barriers and the energy dependence of this tunneling. However, no quantitative theory of PL spectra from p-type δ-doping structures has been developed so far. In fact, such a theory faces serious difficulties, such as the following.

(i) The majority carriers are confined in the δ-doping

well, while the minority carriers are in extended states. To obtain the probabilities of radiative transitions, the states of both types of carriers are required. They may be calculated simultaneously and on the same level of sophistication if the Kane model is used for setting up the effective mass equations. This is not possible if separate models are employed for the two types of carriers, i.e., the Luttinger-Kohn model for holes and a one-band model for electrons.[24–26] In the latter treatment, one first self-consistently solves the effective mass equation for the majority carriers; the self-consistent potential coming out of these calculations is used as external potential in the effective mass equation for the minority carriers, which then is solved without any self-consistency requirement. Using the Kane model, the two steps are done in one. Of course, the results are identical if the $\mathbf{k}\cdot\mathbf{p}$ interaction between conduction and valence bands may be neglected. In GaAs, this interaction affects the electron and light hole states at higher energies[27] but, in our case, its neglect does not appreciably change the results. The main reason why we prefer the Kane model is that the calculations within this model are conceptionally simpler and also applicable to materials with significant $\mathbf{k}\cdot\mathbf{p}$ interaction between conduction and valence bands.

(ii) To solve the multiband effective mass equation, the periodic repetition of the δ-doping layers, i.e., the consideration of δ-doping superlattices (SL's) instead of single δ-doping layers, combined with the representation of the multiband effective mass equation in a plane-wave basis, forms the most general and accurate procedure,[14,15] and we also apply it here. However, to approximate the extended states of isolated δ-doping layers (which most of the experimental results refer to) sufficiently well, the supercells must be rather large, resulting in a rather large plane-wave basis set.

(iii) As the majority carriers form a degenerate gas, each iteration of the self-consistent calculations of carrier states must be performed at all point of a sufficiently fine net of the occupied part of the first SL Brillouin zone (BZ) as in a bulk metal, rather than in special points of the first BZ only as in a bulk semiconductor.

(iv) For the typical doping concentrations, the hole gas of p-type δ-doping structures forms a strongly localized and dense gas. Exchange-correlation effects have been demonstrated to be quite essential in such circumstances.[13,15,16] However, the multicomponent nature of the hole gas makes it impossible to apply the density-functional theory in its standard form; the exchange-correlation potential must be taken as a nondiagonal rather than diagonal matrix with respect to the Bloch basis at the BZ center.

(v) Wave-vector conservation may not *a priori* be assumed for the radiative recombination processes in δ-doping structures. On the contrary, short-range potential fluctuations of the randomly distributed doping atoms make the occurrence of wave-vector nonconserving optical transitions very likely. Thus, both direct and indirect transitions are to be treated.

In the present paper, we solve the above problems and calculate PL spectra for a variety of p-type δ-doping structures. In Sec. II, we describe the calculation method. In Sec. III we demonstrate how the PL spectrum of a prototype SL develops from the self-consistent potential, subband and miniband structures, envelope wave functions, oscillator strengths, and occupation numbers of the SL. In Sec. IV, we provide PL spectra for large period SL's of various sheet doping concentrations and doping spreads, and compare them with experimental PL spectra taken under the same conditions. The comparison shows good agreement for indirect transitions while direct transitions may be ruled out. To account for the experimentally observed strong temperature dependence of the PL spectra, photoinduced minority carrier wells are assumed.

II. METHOD

A. System specification

We consider δ-doping systems specified as follows. The doping layers are taken to be parallel to the (001) plane of GaAs, in accordance with the experimental work we are referring to. The layers are repeated periodically, thus an infinite SL of δ-doping layers is considered rather than an isolated layer. The latter is obtained by taking the limit of large SL period d. The periodic repetition of layers allows us to retain the Bloch character of the eigenstates. If we assume an infinite extension of the SL in all directions, as we will do, periodic boundary conditions may be applied. With an even number of Ga-As bilayers per SL unit cell, the corresponding periodicity region may be taken as tetragonal prism with side length $G_z d$ parallel to the $[001]$ SL axis (which simultaneously forms the z axis of our Cartesian coordinate system), and $G_\parallel(a/\sqrt{2})$ in the two perpendicular directions $[110]$ and $[1\bar{1}0]$; here G_z and $G_\parallel$ are large integers, and a is the host lattice constant.

The one-particle Hamiltonian H of the interacting hole gas of the SL may be written as

$$H = H_0 + V(\mathbf{x}), \tag{1}$$

where H_0 means the one-particle Hamiltonian of the unperturbed bulk crystal and $V(\mathbf{x})$ the perturbation potential induced by the p-type δ doping. For the latter potential one has

$$V(\mathbf{x}) = V_A(\mathbf{x}) + V_H(\mathbf{x}) + V_{\mathrm{XC}}(\mathbf{x}), \tag{2}$$

where $V_A(\mathbf{x})$ is the potential of the ionized acceptor sheets, $V_H(\mathbf{x})$ the Hartree potential, and $V_{\mathrm{XC}}(\mathbf{x})$ the exchange-correlation potential of the interacting hole gas. The hole eigenstates $\psi_\lambda(\mathbf{x},s)$ and eigenenergies E_λ of the SL are determined by the one-particle Schrödinger equation

$$[H_0 + V(\mathbf{x})]\psi_\lambda(\mathbf{x},s) = E_\lambda \psi_\lambda(\mathbf{x},s). \tag{3}$$

To solve this equation, we use effective mass theory.

B. Effective mass theory for δ-doping superlattices

1. Eight-band effective mass equation

Within the eight-band Kane version of effective mass theory, the SL eigenfunctions $\psi_\lambda(\mathbf{x},s)$ are expanded with respect to Bloch states $(\mathbf{x}s|jm_j\mathbf{k})$ of first order $\mathbf{k}\cdot\vec{\pi}$ perturbation theory[25,26] of the $\Gamma_7-\Gamma_8-\Gamma_6$ valence-conduction band complex of the host crystal. The two Γ_7 spin-orbit split

states are identified by $j=\frac{1}{2}$, $m_{1/2}=\pm\frac{1}{2}$, the four Γ_8 heavy- and light-hole band states by $j=\frac{3}{2}$, $m_{3/2}=\pm\frac{3}{2},\pm\frac{1}{2}$, and the two Γ_6 conduction-band states by $j=c$, $m_c=\pm\frac{1}{2}$. The expansion reads

$$\psi_\lambda(\mathbf{x},s)=\sum_{jm_j} F^\lambda_{jm_j}(\mathbf{k})(\mathbf{x}s|jm_j\mathbf{k}), \tag{4}$$

where $F^\lambda_{jm_j}(\mathbf{k})\equiv(jm_j\mathbf{k}|\psi_\lambda)$ are the components of $\psi_\lambda(\mathbf{x},s)$ with respect to the approximate Bloch states $(\mathbf{x}s|jm_j\mathbf{k})$, known as envelope functions. They obey the effective mass equations

$$\sum_{j'm'_j\mathbf{k}'}[\,\delta_{\mathbf{k}\mathbf{k}'}(jm_j\mathbf{k}|H_0|j'm'_j\mathbf{k}) + (jm_j\mathbf{k}|V|j'm'_j\mathbf{k}')]F^\lambda_{j'm'_j}(\mathbf{k}')=\epsilon_\lambda F^\lambda_{jm_j}(\mathbf{k}). \tag{5}$$

The 8×8 matrix $(jm_j\mathbf{k}|H_0|j'm'_j\mathbf{k})$ is given by the expression[25,26]

$$(jm_j\mathbf{k}|H_0|j'm'_j\mathbf{k})=$$

$$\begin{pmatrix}
E_g+Ak^2 & 0 & iP_+ & \sqrt{\frac{2}{3}}P_z & i\sqrt{\frac{1}{3}}P_- & 0 & i\sqrt{\frac{1}{3}}P_z & \sqrt{\frac{2}{3}}P_- \\
0 & E_g+Ak^2 & 0 & -\sqrt{\frac{1}{3}}P_+ & i\sqrt{\frac{2}{3}}P_z & -P_- & i\sqrt{\frac{2}{3}}P_+ & -\sqrt{\frac{1}{3}}P_z \\
-iP_- & 0 & Q & S & R & 0 & \frac{i}{\sqrt{2}}S & -i\sqrt{2}R \\
\sqrt{\frac{2}{3}}P_z & -\sqrt{\frac{1}{3}}P_- & S^* & T & 0 & R & -\frac{i}{\sqrt{2}}(Q-T) & i\sqrt{\frac{3}{2}}S \\
-i\sqrt{\frac{1}{3}}P_+ & -i\sqrt{\frac{2}{3}}P_z & R^* & 0 & T & -S & -i\sqrt{\frac{3}{2}}S^* & -\frac{i}{\sqrt{2}}(Q-T) \\
0 & -P_+ & 0 & R^* & -S^* & Q & -i\sqrt{2}R^* & -\frac{i}{\sqrt{2}}S^* \\
-i\sqrt{\frac{1}{3}}P_z & -i\sqrt{\frac{2}{3}}P_- & -\frac{i}{\sqrt{2}}S^* & \frac{i}{\sqrt{2}}(Q-T) & i\sqrt{\frac{3}{2}}S & i\sqrt{2}R & \frac{1}{2}(Q+T)-\Delta & 0 \\
\sqrt{\frac{2}{3}}P_+ & -\sqrt{\frac{1}{3}}P_z & i\sqrt{2}R^* & -i\sqrt{\frac{3}{2}}S^* & \frac{i}{\sqrt{2}}(Q-T) & \frac{i}{\sqrt{2}}S & 0 & \frac{1}{2}(Q+T)-\Delta
\end{pmatrix}. \tag{6}$$

Here, A is the electron effective mass parameter, Δ is the spin-orbit splitting energy, and E_g the energy gap between conduction and valence bands at Γ. The following abbreviations are used in expression (6):

$$P_\pm=P(k_x\pm ik_y),\quad P_z=Pk_z, \tag{7}$$

$$Q=-\frac{\hbar^2}{2m_0}[(\overline{\gamma_1}+\overline{\gamma_2})(k_x^2+k_y^2)+(\overline{\gamma_1}-2\overline{\gamma_2})k_z^2], \tag{8}$$

$$T=-\frac{\hbar^2}{2m_0}[(\overline{\gamma_1}-\overline{\gamma_2})(k_x^2+k_y^2)+(\overline{\gamma_1}+2\overline{\gamma_2})k_z^2], \tag{9}$$

$$S=i\frac{\hbar^2}{2m_0}2\sqrt{3}\,\overline{\gamma_3}(k_x-ik_y)k_z, \tag{10}$$

$$R=-\frac{\hbar^2}{2m_0}\sqrt{3}[\,\overline{\gamma_2}(k_x^2-k_y^2)-2i\,\overline{\gamma_3}k_xk_z], \tag{11}$$

where $P=-i(\hbar/m_0)(c|p_x|x)$ denotes the Kane matrix element with m_0 being the electron mass, and $\overline{\gamma_1}$, $\overline{\gamma_2}$, $\overline{\gamma_3}$ are the modified Luttinger parameters.[27,28] The latter only account for the $\mathbf{k}\cdot\mathbf{p}$ interaction with remote bands because the interaction between conduction and valence bands is explicitly taken into account in the 8×8 Kane Hamiltonian. In terms of the genuine Luttinger parameters $\gamma_1,\gamma_2,\gamma_3$, the $\overline{\gamma_1}$, $\overline{\gamma_2}$, $\overline{\gamma_3}$ are expressed as[28]

$$\overline{\gamma_1}=\gamma_1-\frac{1}{3}\frac{E_p}{E_g},\quad \overline{\gamma_2}=\gamma_2-\frac{1}{6}\frac{E_p}{E_g},\quad \overline{\gamma_3}=\gamma_3-\frac{1}{6}\frac{E_p}{E_g}, \tag{12}$$

with $E_p=(2m_0/\hbar^2)P^2$ as Kane energy. Because of the independence of the potential $V(\mathbf{x})$ of the position vector component parallel to the layers and because of the SL periodicity of $V(z)$, the envelope function $F^\lambda_{jm_j}(\mathbf{x})$ may be written as the product of a plane wave with wave vector $\mathbf{q}_\parallel$ parallel to the layers, and a z-dependent Bloch function of the SL defined by a quasi-wave-vector q_z of the first SL BZ and a certain SL band index ν. Thus, setting $\lambda=\nu\mathbf{q}$, $\mathbf{q}=(\mathbf{q}_\parallel,q_z)$, the envelope functions $F^{\nu\mathbf{q}}_{jm_j}(\mathbf{x})$ in $\mathbf{k}$ space read as

$$F^{\nu\mathbf{q}}_{jm_j}(\mathbf{k})=\delta_{\mathbf{k}\mathbf{q}+K\mathbf{e}_z}F^{\nu\mathbf{q}}_{jm_j}(K), \tag{13}$$

where K means a vector of the reciprocal SL, and $\mathbf{e}_z$ a unit vector in the z direction. The Fourier coefficients $F^{\nu\mathbf{q}}_{jm_j}(K)$ of the SL Bloch function are determined by the effective mass equation (5), which results in

$$\sum_{j'm_j'}\sum_{K'}[\,\delta_{KK'}(jm_j\mathbf{q}+K\mathbf{e}_z|H_0|j'm_j'\mathbf{q}+K'\mathbf{e}_z)+(jm_j\mathbf{q}+K\mathbf{e}_z|V|j'm_j'\mathbf{q}+K'\mathbf{e}_z)]F^{\nu\mathbf{q}}_{j'm_j'}(K')=E_{\nu\mathbf{q}}F^{\nu\mathbf{q}}_{jm_j}(K). \tag{14}$$

2. Coulomb potential

Within effective mass theory, the Coulomb part $V_A(z)+V_H(z)$ of the total perturbation potential $V(z)$ has vanishing off-diagonal elements $(jm_jK|V_A+V_H|j'm_j'K')$ with respect to $jm_j, j'm_j'$, hence

$$(jm_jK|V_A+V_H|j'm_j'K')=\delta_{jj'}\delta_{m_jm_j'}(K|V_A+V_H|K'), \tag{15}$$

where $(K|V_A+V_H|K')\equiv(K-K'|V_A+V_H)$ denotes the Fourier coefficients of $V_A(z)+V_H(z)$. The latter are determined by Poisson's equation,

$$(K|V_A+V_H|K')=-\frac{4\pi e^2}{\epsilon}\frac{1}{|K-K'|^2}(K|p-N_A|K'). \tag{16}$$

Here ϵ denotes the static dielectric constant of bulk GaAs, and $p(z)$ is the hole concentration averaged with respect to a primitive unit cell. One has

$$p(z)=\frac{1}{\Omega}\sum_{\nu\mathbf{q}}\sum_{KK'}\sum_{jm_j}e^{i(K-K')z}F^{\nu\mathbf{q}*}_{jm_j}(K')F^{\nu\mathbf{q}}_{jm_j}(K)\times\left[1-\frac{1}{e^{[E_{\nu\mathbf{q}}-E_F]/kT}+1}\right], \tag{17}$$

where E_F is the Fermi energy of the confined hole gas. The distribution of N_A of the ionized dopant atoms along the SL axis is approximated by a sum of Gaussians,

$$N_A(z)=N_s\sum_{n=-\infty}^{\infty}\frac{1}{\sqrt{2\pi}\sigma}e^{-(z-nd)^2/2\sigma^2}, \tag{18}$$

where N_s means the sheet doping concentration of a doping layer, and σ^2 is the variance of the Gaussian distribution. It determines the full width Δz at half-maximum of the Gaussian by means of the relation $\Delta z=2\sqrt{2\,ln2}\,\sigma=2.355\sigma$.

3. Exchange-correlation potential

The exchange-correlation potential matrix $(jm_j\mathbf{k}K|V_{\rm XC}|j'm_j'\mathbf{k}K')$ has off-diagonal elements both with respect to jm_j, $j'm_j'$, and K,K'. Neglecting any exchange-correlation-induced couplings between the three groups of carriers involved, i.e., electrons, heavy and light holes, and spin-orbit-split holes, the (8×8) exchange-correlation matrix decomposes into (2×2) blocks for electrons and spin-orbit-split holes, and a (4×4) block for heavy and light holes. For p-type δ-doping SL's in GaAs, the densities of electrons and spin-orbit-split holes are negligibly small. Thus, only the (4×4) block of the exchange-correlation potential matrix is nonzero. In local-density approximation, the elements of this matrix may be expressed in terms of the local exchange-correlation potentials $V^{\rm hh}_{\rm XC}(z)$ and $V^{\rm lh}_{\rm XC}(z)$ of heavy and light holes, respectively, as has been demonstrated in Refs. 15,16. To obtain $V^{\rm hh}_{\rm XC}(z)$ and $V^{\rm lh}_{\rm XC}(z)$, the parameterized expressions derived by Hedin and Lundquist[29] in the case of a homogeneous electron gas are adopted for the homogeneous gas of heavy and light holes. The exchange interaction is taken into account only between holes of the same type, while correlation is considered also between heavy and light holes.

In solving the effective mass equation (14), both the Coulomb potential and the exchange-correlation potential are treated self-consistently.

C. Luminescence spectrum

1. General expression

The emission of light from a p-type δ-doping SL is due to spontaneous radiative recombination processes between optically excited nonequilibrium electrons and equilibrium holes. Both electrons and holes are in Bloch-type SL eigenstates $\nu\mathbf{q}$. All states are twofold degenerate because of time-reversal symmetry combined with spatial-inversion symmetry. We account for the degeneracy by setting $\nu=n\sigma$, where $n=1,2,3\ldots$, labels the different minibands, and σ is a ''spin quantum number'' with the two values $\uparrow$ and $\downarrow$, distinguishing the two Bloch states of a given band. To separate between Bloch states $n\sigma\mathbf{q}$ for electrons and holes, we add an index e' for electrons, hh$'$ for heavy holes and lh$'$ for light holes, i.e., we write $\nu_e\sigma_e\mathbf{q}_e$, $\nu_{\rm hh}\sigma_{\rm hh}\mathbf{q}_{\rm hh}$, $\nu_{\rm lh}\sigma_{\rm lh}\mathbf{q}_{\rm lh}$. Spin-orbit-split hole states are not needed for the calculation of luminescence spectra since these are not populated. Assuming direct optical transitions, with $\mathbf{q}_e=\mathbf{q}_{th}\equiv\mathbf{q}$, $t=h,l$, the luminescence intensity $I(\omega)$ of the SL may be written as[30]

$$I(\omega)=\frac{2\hbar\omega^3}{c}\frac{e^2}{m_0c^2}\sum_{\mathbf{q}}\sum_{n_e}\sum_{t=l,h}\sum_{n_{th}}f_{n_en_{th}}(\mathbf{q})N_{n_e\mathbf{q}}\times[1-N_{n_{th}\mathbf{q}}]\left(\frac{1}{\pi}\right)\times\frac{\gamma_{n_en_{th}}}{[E_{n_e}(\mathbf{q})-E_{n_{th}}(\mathbf{q})-\hbar\omega]^2+\gamma^2_{n_en_{th}}} \tag{19}$$

Here, $N_{n_e\mathbf{q}}$ and $[1-N_{n_{th}\mathbf{q}}]$ denote the electron and hole occupation probabilities, respectively, $\gamma_{n_en_{th}q}$ is the lifetime broadening energy, and $f_{n_en_{th}}(\mathbf{q})$ the oscillator strength of an electron-hole transition, given by the relation

$$f_{n_en_{th}}(\mathbf{q})=\frac{2}{m_0}\sum_{\sigma_e\sigma_{th}}\frac{|(n_e\sigma_e\mathbf{q}|p_x|n_{th}\sigma_{th}\mathbf{q})|^2}{E_{n_e}(\mathbf{q})-E_{n_{th}}(\mathbf{q})}. \tag{20}$$

2. Oscillator strengths

Using expressions (4) and (13) for the SL eigenstates $(s\mathbf{x}|\nu\mathbf{q})$, the momentum matrix elements $(n_e\sigma_e\mathbf{q}|p_x|n_{th}\sigma_{th}\mathbf{q})$ entering the oscillator strength (20) may be written as

$$(n_e\sigma_e\mathbf{q}|p_x|n_{qh}\sigma_{qh}\mathbf{q})$$
$$=G^3\sum_K\sum_{jm_j}\sum_{j'm_j'}F^{n_e\sigma_e\mathbf{q}*}_{j'm_j'}(K)F^{n_{th}\sigma_{th}\mathbf{q}}_{jm_j}(K)(j'm_j'|p_x|jm_j), \tag{21}$$

with $G^3=G_zG_\parallel^2$. In evaluating expression (21) we may use the fact that, in the case of GaAs, the conduction band is only weakly coupled to any valence band, and the two heavy- and light-hole bands do only weakly interact with the spin-orbit-split band. Thus we have approximately

$$F^{n_e\sigma_e\mathbf{q}}_{(3/2)m_{3/2}}(K)=F^{n_e\sigma_e\mathbf{q}}_{(1/2)m_{1/2}}(K)=0, \tag{22}$$

$$F^{n_{th}\sigma_{th}\mathbf{q}}_{cm_c}(K)=F^{n_{th}\sigma_{th}\mathbf{q}}_{(1/2)m_{1/2}}(K)=0, \quad t=l,h. \tag{23}$$

The only momentum matrix elements that occur as factors at nonvanishing wave-function components are those of the form $(cm_c|p_x|\frac{3}{2}m_{3/2})$. Using the expansion of the Bloch functions $|\frac{3}{2}m_{3/2})$ at Γ with respect to the basis functions $|x)|\uparrow),|x)|\downarrow),|y)|\uparrow),\ldots,|z)|\downarrow)$,[26] these elements may be expressed in terms of the Kane matrix element $P=-i(\hbar/m_0)(c|p_x|x)$ as follows:

$$(c\tfrac{1}{2}|p_x|\tfrac{3}{2}\tfrac{3}{2})=\frac{1}{\sqrt{2}}P, \quad (c\overline{\tfrac{1}{2}}|p_x|\tfrac{3}{2}\overline{\tfrac{1}{2}})=\frac{i}{\sqrt{2}}P, \tag{24}$$

$$(c\tfrac{1}{2}|p_x|\tfrac{3}{2}\overline{\tfrac{1}{2}})=\frac{1}{\sqrt{6}}P, \quad (c\overline{\tfrac{1}{2}}|p_x|\tfrac{3}{2}\tfrac{1}{2})=\frac{i}{\sqrt{6}}P, \tag{25}$$

$$(c\tfrac{1}{2}|p_x|\tfrac{3}{2}\tfrac{1}{2})=(c\overline{\tfrac{1}{2}}|p_x|\tfrac{3}{2}\overline{\tfrac{1}{2}})=0, \tag{26}$$

$$(c\tfrac{1}{2}|p_x|\tfrac{3}{2}\overline{\tfrac{3}{2}})=(c\overline{\tfrac{1}{2}}|p_x|\tfrac{3}{2}\tfrac{3}{2})=0. \tag{27}$$

Not all of the elements $(n_e\sigma_e\mathbf{q}|p_x|n_{th}\sigma_{th}\mathbf{q})$ are independent; one has

$$|(n_e\uparrow\mathbf{q}|p_x|n_{th}\uparrow\mathbf{q})|^2=|(n_e\downarrow\mathbf{q}|p_x|n_{th}\downarrow\mathbf{q})|^2, \quad t=l,h \tag{28}$$

$$|(n_e\downarrow\mathbf{q}|p_x|n_{th}\uparrow\mathbf{q})|^2=|(n_e\uparrow\mathbf{q}|p_x|n_{th}\downarrow\mathbf{q})|^2, \quad t=l,h. \tag{29}$$

For the independent elements one obtains

$$|(n_e\uparrow\mathbf{q}|p_x|n_{th}\uparrow\mathbf{q})|^2=G^3\frac{P^2}{2}\left|\sum_K F^{n_e\uparrow\mathbf{q}*}_{1\,c\frac{1}{2}}(K)\left(F^{n_{th}\uparrow\mathbf{q}}_{3\frac{3}{2}\frac{3}{2}}(K)+\frac{1}{\sqrt{3}}F^{n_{th}\uparrow\mathbf{q}}_{31\overline{\frac{2}{2}}}(K)\right)\right|^2, \tag{30}$$

$$|(n_e\downarrow\mathbf{q}|p_x|n_{th}\uparrow\mathbf{q})|^2=G^3\frac{P^2}{2}\left|\sum_K F^{n_e\downarrow\mathbf{q}*}_{\overline{1}\,c\frac{1}{2}}(K)\left(F^{n_{th}\uparrow\mathbf{q}}_{33\overline{\frac{2}{2}}}(K)+\frac{1}{\sqrt{3}}F^{n_{th}\uparrow\mathbf{q}}_{3\frac{1}{2}\frac{1}{2}}(K)\right)\right|^2. \tag{31}$$

Using these results, the oscillator strength $f_{n_en_{th}}(\mathbf{q})$ of an electron-to-hole transition may be expressed as

$$f_{n_en_{th}}(\mathbf{q})=\frac{4}{m_0[E_{n_e}(\mathbf{q})-E_{n_{th}}(\mathbf{q})]}[|(n_e\uparrow\mathbf{q}|p_x|n_{th}\uparrow\mathbf{q})|^2+|(n_e\downarrow\mathbf{q}|p_x|n_{th}\uparrow\mathbf{q})|^2]. \tag{32}$$

3. Indirect transitions

The ionized impurity potential V_A of δ-doping structures exhibits fluctuations on the atomic length scale. These may result in indirect optical transitions. The luminescence intensity of such transitions may formally be obtained from expressions (19) and (20) for direct transitions by replacing the electron $\mathbf{q}$ vector by $\mathbf{q}_e$ and the hole $\mathbf{q}$ vector by $\mathbf{q}_{th}$. This results in

$$I(\omega)=\frac{2\hbar\omega^3}{c}\frac{e^2}{m_0c^2}\sum_{\mathbf{q}_e\mathbf{q}_e}\sum_{n_e}\sum_{t=l,h}\sum_{n_{th}}f_{n_en_{th}}(\mathbf{q}_e,\mathbf{q}_h)N_{n_e\mathbf{q}_e}\times[1-N_{n_{th}\mathbf{q}_{th}}]\left(\frac{1}{\pi}\right)\times\frac{\gamma_{n_en_{th}}}{[E_{n_e}(\mathbf{q}_e)-E_{n_{th}}(\mathbf{q}_{th})-\hbar\omega]^2+\gamma^2_{n_en_{th}}}, \tag{33}$$

$$f_{n_en_{th}}(\mathbf{q}_e,\mathbf{q}_{th})=\frac{2}{m_0}\sum_{\sigma_e\sigma_{th}}\frac{|(n_e\sigma_e\mathbf{q}_e|p_x|n_{th}\sigma_{th}\mathbf{q}_{th})|^2}{E_{n_e}(\mathbf{q}_e)-E_{n_{th}}(\mathbf{q}_{th})}. \tag{34}$$

In evaluating the oscillator strength $f_{n_en_{th}}(\mathbf{q}_e,\mathbf{q}_{th})$, a wave-vector-conserving factor $\delta_{\mathbf{q}_e\mathbf{q}_{th}}$ occurs. We replace this factor by unity, accounting for scattering from short-range potential fluctuations in this way.

In the section that follows, we apply the above formalism to a special SL and demonstrate how its PL spectrum evolves from the various quantities determining it: the self-consistent potential, the subband and miniband structures, the envelope functions, oscillator strengths, and occupation numbers.

III. FORMATION OF THE PL SPECTRUM FOR A PROTOTYPE *P*-TYPE δ-DOPING SL

The special SL considered here has a sheet doping concentration $N_s=8\times10^{12}$ cm^{-2}, a doping spread $\Delta z=23.5$ Å, and a SL period $d=500$ Å. The parameters of the Kane model for GaAs are taken as follows:[31] $m_e=0.0665$ $\gamma_1=6.790$, $\gamma_2=1.924$, $\gamma_3=2.780$, $E_p=29.12$ eV. The energy gap $E_g(0)$ at $T=0$ K is 1.519 eV, and its temperature dependence $E_g(T)$ is taken from the relation $E_g(T)=E_g(0)+5.405\times10^{-4}T^2/(204+T)$.[32]

A. Self-consistent potential

As shown in Fig. 1, the self-consistent potential differs for the three types of particles involved, being the electrons, heavy holes, and light holes. The difference is due to the exchange-correlation part of the potential. For electrons and spin-orbit-split holes, this potential part vanishes because the densities of these particles are negligibly small in the *p*-type

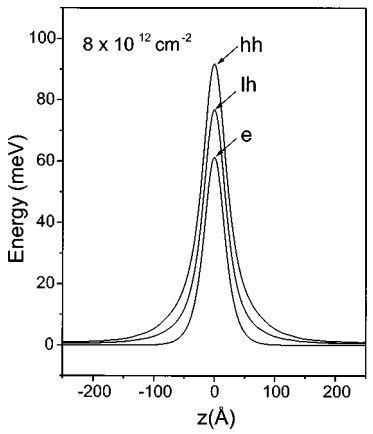

FIG. 1. Self-consistent potentials for electrons, heavy holes, and light holes of a p-type δ-doping SL. Sheet doping concentration $N_s = 8\times10^{12}$ cm^{-2}, doping spead $\Delta z = 23{,}5$ Å, and SL period $d = 500$ Å.

δ-doping SL under consideration. For holes, the exchange-correlation potential is essentially nonzero; its difference for heavy and light holes is due to the different masses and densities of these particles (a detailed analysis of exchange-correlation effects in p-type δ-doping SL's is given elsewhere[15,16]).

B. Envelope functions

While the holes see the potential region of a δ-doping layer as a well, it is seen as a barrier by the electrons. The region *between* the layers forms a barrier for holes and a well for electrons. For both types of carriers, the envelope functions are Bloch functions $(z|n_{e/th}q_z)$ perpendicular to the layers and plane waves $\exp[i\mathbf{q}_\parallel\cdot\mathbf{x}_\parallel]$ parallel to the layers. The probability distributions $|(z|n_{e/th}q_z=0)|^2$, taken at the center Γ of the first SL BZ, are depicted in Fig. 2. For holes below the barriers, they are essentially nonzero within the (hole) well regions, while they decay exponentially into the (hole) barriers between the layers. The probability distributions for electrons are large between the layers, and decay exponentially into the well regions.

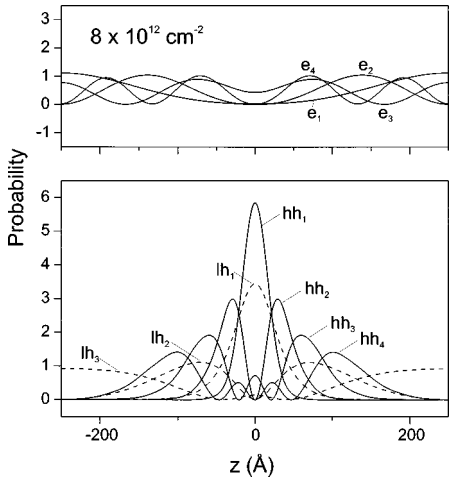

FIG. 2. Probability distributions of electrons and holes for various subband levels at the first SL BZ center for the same p-type δ-doping SL as in Fig. 1.

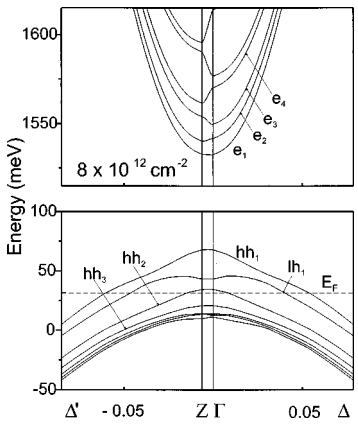

FIG. 3. Subband and miniband dispersions of electrons and holes for the same p-type δ-doping SL as in Fig. 1.

C. Band structure

The miniband and subband structures of the SL are shown in Fig. 3 for holes (lower part) and for electrons (upper part). The dispersion $E_{n_{th}\sigma_{th}}(\mathbf{k}_\parallel,0)$ of the hole subbands parallel to the layers exhibits the typical anticrossing behavior. The miniband dispersion $E_{n_{th}\sigma_{th}}(\mathbf{0}_\parallel,k_z)$ for holes is rather small, because of the large barrier width. Two hole subbands, the lowest for heavy holes (hh1) and the lowest for light holes (lh1), are partially occupied in the case under consideration.

To understand the electron band structure in Fig. 3, one has to realize that the width of the electron wells is given by the SL period, which here is much larger than the width of the hole wells. Thus, the electron minibands $E_{n_e\sigma_e}(\mathbf{0}_\parallel,k_z)$ of the SL are much wider and the minigaps much smaller than those of holes. For isolated δ-doping layers, i.e., for SL periods tending to infinity, the width $(2\pi/d)$ of the first SL BZ shrinks to zero and, simultaneously, the electron minibands transform into a continuous energy spectrum without minigaps. To approximate an isolated δ well by a SL of such wells, the minigaps of the latter should be small compared to the lifetime broadening energies $\gamma_{n_e n_{th}}$ of the transitions involved, which typically are several meV. For the period of 500 Å shown in Fig. 3 this condition is not yet fulfilled, one has to go up to $d = 2000$ Å to avoid artificial electron confinement effects.

D. Oscillator strengths

Knowing the electron and hole band structures and eigenfunctions, one is able to calculate the direct and indirect PL spectra $I(\omega)$ by means of expressions (19) and (33), respectively. The eigenfunctions enter these expressions through the oscillator strength $f_{n_e n_{th}}(\mathbf{k})$ of a radiative electron-hole recombination process defined in Eqs. (20) and (34). The oscillator strength is shown in Fig. 4 for direct transitions from electron states to the two lowest heavy-hole states and the two lowest light-hole states at the first SL BZ center Γ. Actually, $f_{n_e 1_{th}}(\mathbf{0})$, $t=h,l$, is plotted against the electron energy $E_{n_e}(\mathbf{0})$ of the various minibands n_e at Γ.

For transitions to the heavy-hole ground state hh1, $f_{n_e 1_{\rm hh}}(\mathbf{0})$ steeply increases between the first and second electron miniband reaching a maximum at the latter. From the

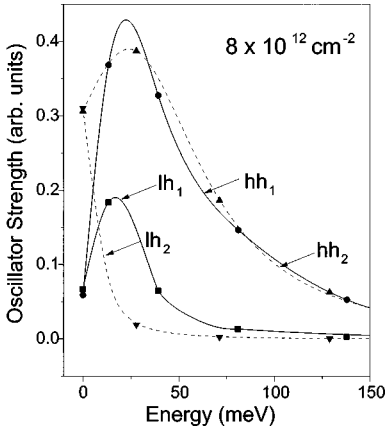

FIG. 4. Oscillator strengths for optical transitions from electron states to the heavy- and light-hole ground states at the first SL BZ center, plotted against the electron energy. The same p-type δ-doping SL is considered as in Fig. 1.

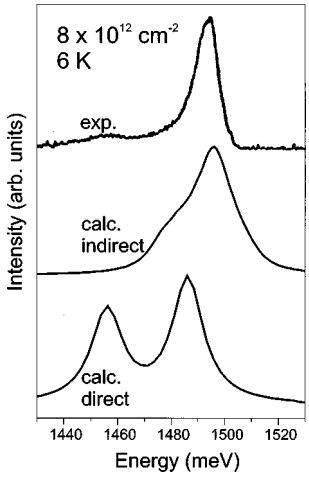

FIG. 5. Calculated PL spectra for the p-type δ-doping SL of Fig. 1. Lifetime broadening energy 5 meV. A measured spectrum taken in Ref. 8 from the same SL is shown for comparison.

second miniband on, $f_{n_e 1_{\rm hh}}(\mathbf{0})$ decreases continuously. This behavior reflects the variation of the spatial overlap of the electron and hole envelope functions: for low electron energies, the electron wave function decays rapidly into the hole wells, and the overlap is small. With growing energy, the electron penetration into the hole well increases, and the overlap becomes larger. If the energy of the electron grows further, its wave function oscillates more rapidly and the integrand of the overlap integral is averaged out more effectively.

For transitions to the light-hole ground state lh1, the oscillator strength $f_{n_e 1_{\rm lh}}(\mathbf{0})$ exhibits qualitatively the same behavior as in the heavy-hole case. For the lowest electron miniband, $f_{n_e 1_{\rm lh}}(\mathbf{0})$ has almost the same value as $f_{n_e 1_{\rm hh}}(\mathbf{0})$. This is remarkable since the squares of the momentum matrix elements between conduction- and valence-band bulk states, entering the oscillator strength of Eq. (20), is three times larger for heavy holes than for light holes. In a SL, the oscillator strengths of light holes are enhanced because the latter penetrate deeper into the barriers than heavy holes. For the second electron miniband, the oscillator strength of light-hole transitions is half of that for heavy-hole transitions. With increasing electron miniband number, the light holes rapidly lose intensity with respect to the heavy holes. This is due to the above-discussed partial averaging out of the integrand of the overlap integral, which is more effective for the moderately localized light-hole wave functions than for the strongly localized heavy-hole wave functions (see Fig. 2).

The oscillator strengths for transitions to the first excited heavy-hole state hh2 exhibits qualitatively the same energy dependence as that for transitions to the heavy-hole ground state. The absolute values are larger for the hh2 transitions than for the hh1 transitions, reflecting the enhanced penetration of the hh2 state into the barrier. The same statements hold for transitions to the first excited light-hole state lh2 in comparison with transitions to the light-hole ground state lh1.

E. Occupation numbers

To calculate PL spectra $I(\omega)$ according to expressions (19) and (33), the electron and hole occupation numbers $N_{n_e \mathbf{k}}$ and $[1-N_{n_{th}\mathbf{k}}]$ are needed. Considering low excitation densities, the photoexcited electrons may be assumed to be completely thermalized and their occupation numbers to be given by the Boltzmann distribution function,

$$N_{n_e \mathbf{k}} = e^{[E_{Fn}-E_{n_e}(\mathbf{k})]/kT}. \tag{35}$$

The quasi-Fermi energy E_{Fn} entering here is numerically calculated by normalizing the Boltzmann distribution. The hole occupation numbers $[1-N_{n_{th}\mathbf{k}}]$ are governed by the Fermi distribution function,

$$[1-N_{n_{qh}\mathbf{k}}] = \frac{1}{e^{[(E_F-E_{n_{qh}}(\mathbf{k})]/kT}+1}. \tag{36}$$

F. PL spectra

PL spectra of the SL under consideration are shown in Fig. 5, once calculated for direct transitions and once for indirect transitions. The temperature is taken to be $T=6$ K in both cases, and the lifetime broadening energy is set to 5 meV. The spectrum for direct transitions shows two peaks below the gap. These are clearly due to electron transitions to confined hole states close to Γ, the low-energy peak corresponding to the hh1 band, and the high-energy peak to the lh1 band, which are the only SL bands partially occupied by holes in the present case (see Fig. 3). The light-hole peak is stronger than the heavy-hole peak. A look at the oscillator strengths in Fig. 4 reveals the reason for this uncommon behavior: the average electron energy kT, counted from the lowest band bottom, is as small as 0.5 meV at $T=6$ K. For such small electron energies, the oscillator strengths for transitions to heavy and light holes are almost equal. The splitting between the two PL peaks is 30 meV, which is 5 meV larger than the energy separation between the lowest heavy- and light-hole bands at Γ (see Fig. 3).

The PL spectrum for indirect transitions in Fig. 5 looks qualitatively different. The heavy- and light-hole peaks of the direct spectrum are absent, and instead a broad asymmetric peak occurs with a shoulder on its low-energy side, at roughly the position of the lh1 peak of the direct spectrum.

The peak is due to indirect recombination processes of electrons close to Γ with hh1 and lh1 holes having any wave vector below the Fermi surface. The low-energy shoulder is seen because the wave-vector dispersion of the lh1 band is rather flat (see Fig. 3). In Fig. 5 we also show an experimental spectrum for a sample of sheet doping concentration 8×10^{12} cm^{-2} and a temperature of 6 K (the doping spread of the sample was not measured). This spectrum in Fig. 5 has been taken from a series of experimental spectra reported in Ref. 18 for different excitation powers. We show the spectrum with the lowest excitation power (3 mW/cm^2), which should be the closest one to our calculations, which assume low excitation densities. Comparing the experimental and theoretical spectra one notices that the calculated spectrum for indirect transitions fits much better than the spectrum for direct transitions. This remains true if one enlarges the doping spread and/or the lifetime broadening parameter $\gamma_{n_e n_{th}}$ in the calculations. Thus, we conclude that the dominating radiative recombination processes in the measured sample are indirect rather than direct transitions.

IV. PL SPECTRA FOR VARIOUS *P*-TYPE δ-DOPING SL'S AND COMPARISON WITH EXPERIMENT

Below, we present calculated PL spectra of p-type δ-doping structures for which experimental PL spectra are available for comparison. We also discuss the temperature dependence of the overall PL intensity which, in experiment, has been found to be extraordinary strong in certain circumstances. From various reasons, the agreement between theory and experiment cannot be expected to be complete. For example, the experimental doping spread Δz (provided it is measured at all) has considerable uncertainties, while it is known that the hole band-structure sensitively depends on Δz.[12,13,15] The calculated potential well may differ somewhat from the experimental one because of the Fermi-level pinning at the surface and because of a homogeneous background doping of the sample. The parameters entering the PL spectra, like the energy gap E_g or the lifetime broadening energy, change with excitation power and temperature T. The T dependence of E_g is well known for GaAs,[32] and may easily be included in the calculations. Other dependencies are only poorly known for the systems under consideration and can only qualitatively be discussed. We concentrate on the effects that the confined hole structure has on the PL spectra. These are rigorously treated in our calculations.

A. Variation of sheet doping concentration

The samples considered in this subsection are close to those shown in Fig. 4 of Ref. 12. In the measurements,[12] a single δ layer was embedded between two $Ga_{67}Al_{33}As$ barriers in a distance of 300 Å on each side. The sheet doping concentrations and doping spreads were varied: $N_s=3\times10^{12}$, $\Delta z=65$ Å for sample 2, $N_s=8\times10^{12}$, $\Delta z=72$ Å for sample 3, $N_s=3\times10^{13}$, $\Delta z=125$ Å for sample 4. In the calculations, the barriers are simulated by δ wells, using SL's of period $d=600$ Å. The following hole levels are occupied: hh1 and lh1 for sample 2, hh1, lh1, and hh2 for sample 3, and hh1, lh1, hh2, hh3, lh2, lh3, and hh4 for sample 4. The large number of occupied bands of sample 4 is due to the heavy doping combined with the wide doping spread.

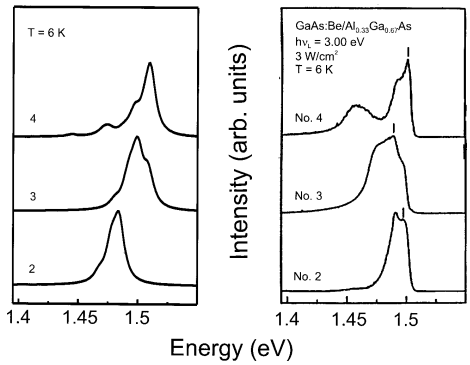

FIG. 6. Calculated PL spectra (left-hand side) for p-type δ-doping SL's of $d=500$ Å having sheet doping concentrations N_s and doping spreads Δz as follows: sample 2, 3×10^{12} cm^{-2}, 6.5 nm; sample 3, 8×10^{12} cm^{-2}, 7.2 nm; sample 4, 3×10^{13} cm^{-2}, 12.5 nm. Temperature 6 K, lifetime broadening energy 5 meV. On the right-hand side, experimental spectra measured in Ref. 12 on the same samples are shown for comparison.

Again, the calculated spectra for direct transitions considerably differ from the experimental ones. The indirect spectra are shown in Fig. 6, left-hand side. For sample 2, one has a single peak caused by transitions to hh1 and lh1 holes. For sample 3, one observes one peak having a shoulder on its high-energy side. The peak is again due to the hh1 and lh1 holes, while the shoulder results from the hh2 holes. The two former structures exist also in sample 4. In addition, a new strong peak develops at higher energies. It is due to hh3, lh2, lh3, and hh4 holes. The weak structure on the low-energy side of the spectrum is caused by transitions to hh1 holes in the vicinity of Γ, which give rise to notable emission because of their relatively large density of states.

The experimental spectra of the three samples[12] taken at $T=6$ K, are shown on the right-hand side of Fig. 6. The Fermi-level enhancement seen in the measured spectra is not reproduced in our calculations because the excitonlike many-body effects at the Fermi level[33] were not included. Moreover, the main peaks of the three experimental spectra appear at almost the same energy, while the main peaks of the calculated spectra shift towards higher energies with rising doping concentrations. We attribute this difference to the shrinkage of the energy gap for samples with heavier doping. Employing this interpretation, we estimate a gap shrinkage of 50 meV between $N_s=3\times10^{12}$ and $N_s=3\times10^{13}$. This value compares well with the experimental gap shrinkage reported in Refs. 34 and 35 for p-type bulk GaAs. Correcting the calculated spectra of Fig. 6 for the Fermi-level enhancement and the gap shrinkage, they compare fairly well with the experimental spectra in this figure. The fact that the low-energy peak of sample 4 is more pronounced in the experimental spectrum than in the theoretical one could be due to the simulation of the $Ga_{0.67}Al_{0.33}As$ barriers by δ-doping wells in our calculations. This renders the confinement less effective and diminishes the low-energy peaks.

B. Temperature dependence of PL spectra

An interesting question which has not been addressed so far is the variation of the PL spectra with temperature. Figure

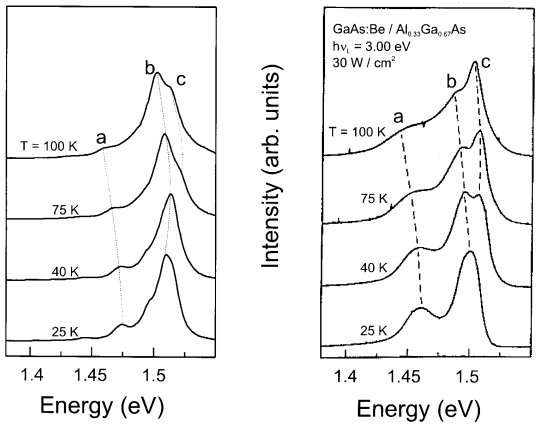

FIG. 7. Temperature-dependent PL spectra for sample 4 of Fig. 6. The calculated spectra are shown on the left-hand side, and the experimental spectra of Ref. 12 are displayed on the right-hand side. The spectra are normalized with respect to their absolute maxima. Lifetime broadening energy is 5 meV in the calculations.

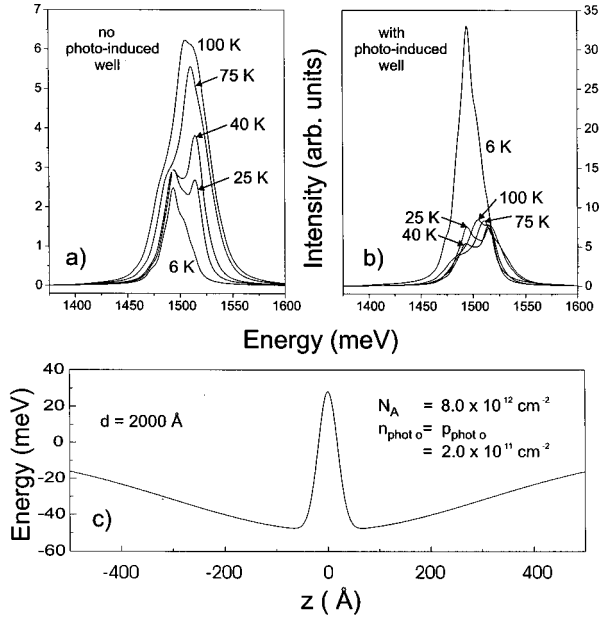

FIG. 8. In part (a), calculated PL spectra are shown at various temperatures for a p-type δ-doping SL with $N_s=8\times10^{12}$ cm^{-2}, $\Delta z=23.5$ Å, $d=2000$ Å. Lifetime broadening energy 5 meV. The spectra are not normalized. In part (b), indirect PL spectra are shown for the same SL, but assuming a photoinduced net charge density $p_{\text{photo}}=2\times10^{11}$ cm^{-2} of the hole well. The potential well of the latter structure is shown in part (c). It clearly reveals the photoinduced well for electrons.

7 shows calculated and measured PL spectra at various temperatures for a sample with $N_s=3\times10^{13}$, $\Delta z=125$ Å, and $d=500$ Å. The sample parameters are the same as those of sample 4 in Fig. 6. Thus, seven hole bands are partially occupied, being hh1, lh1, hh2, hh3, lh2, lh3, and hh4. The spectra on the left-hand side of Fig. 7 have been calculated assuming indirect transitions, and a lifetime broadening energy of 5 meV. The low-energy peak labeled as (a) shifts down and loses intensity if the temperature increases. This peak is due to transitions into the heavy- and light-hole ground-state levels hh1, lh1. The weak (unlabeled) structure between peaks a and b seen in the two calculated low-temperature spectra results from hh2 transitions. The main peak of the spectra labeled as b is due to hh3, lh2, lh3, and hh4 holes. It moves up between 25 K and 40 K, and down between 40 K and 100 K. A third peak labeled as c appears at 75 K and moves down if T rises up to 100 K. The down shifts of the three peaks a, b, and c are due to the lowering of the energy gap with rising temperature. Peak c stems mainly from the recombination of electrons, which are thermally excited at higher temperature. This may be understood by means of Fig. 4, which shows that the oscillator strengths for hh1, lh1, and hh2 transitions increase with rising thermal energy kT. To a minor part, the additional high-temperature peak is due to holes excited into bands above the Fermi level. Although far fewer holes are excited than electrons owing to the degeneracy of the hole gas, the contribution of the excited holes is notable because of their large oscillator strengths.

The experimental spectra shown on the right-hand side of Fig. 7 are those from Fig. 8 of Ref. 12. The labeled peaks a, b, and c of the calculated spectra are also seen in the measured spectra. They are more pronounced than in the calculated spectra, which again could be due to the simulation of the $Ga_{67}Al_{33}As$ barriers by δ-doping wells in our calculations. The temperature behavior of the experimental peaks is close, although not equal, to that of the calculated peaks.

In Fig. 7, the spectra are normalized with respect to their largest peaks, respectively, i.e., no attention is paid to the actual intensities at various temperatures. This is done in Fig. 8. On the left-hand side of this figure we illustrate the temperature dependence of the indirect PL spectra of a SL with $N_s=8\times10^{12}$, $\Delta z=23.5$ Å, and $d=2000$ Å. The large period of the SL guarantees isolated hole wells and, what turns out to be more critical, practically unconfined electrons. For the sample under consideration, the hh1, lh1, and hh2 hole bands are partially occupied. Each spectrum on the left-hand side of Fig. 8 exhibits a structured emission band, caused by transitions to the three hole bands hh1, lh1, and hh2 at all wave vectors below the Fermi surface. The Q2D emission band grows and broadens towards higher energies if the temperature increases. The reason already has been discussed above: Rising the temperature, electrons are excited from states at lower energies to states at higher energies. Transitions from high-energy electron states to the confined heavy- and light-hole states have larger oscillator strengths than transitions from low-energy states, thus the Q2D emission band gains intensity and its center of gravity shifts to higher energies, as seen in the left-hand part of Fig. 8.

Experimentally, just the opposite behavior is observed, the Q2D hole emission band loses intensity if the temperature rises. This may be seen in Fig. 9(a), which shows the PL spectra of an isolated p-type δ-doping well measured in Ref. 19 at various temperatures under an excitation of 100 W/cm^2 (note that the energy scale is reversed, and the intensity is plotted on a logarithmic scale). The peaks labeled as A are due to the bound exciton recombination of bulk GaAs. This recombination channel is not included in our calculations, thus, no equivalent of peak A exists in the spectra of Fig. 8. On the low-energy side of peak A, the Q2D emission band occurs in each experimental spectrum of Fig. 9(a). The intensity of the bound exciton peak A decreases by about two orders of magnitude if the temperature rises from 2 to 60 K.

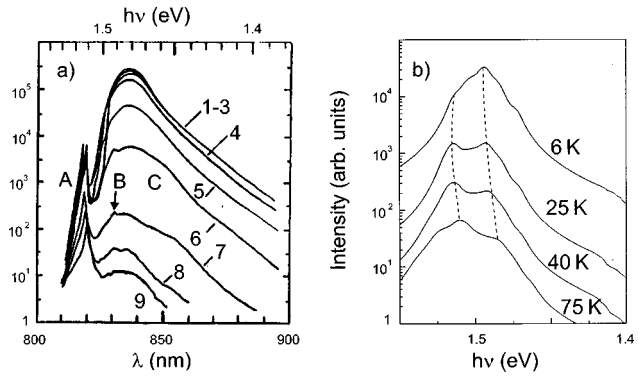

FIG. 9. Temperature-dependent PL spectra (unnormalized) of an isolated p-type δ-doping well with $N_s = 3.9 \times 10^{12}$ cm^{-2}. Part (a) shows the experimental spectra of the well taken in Ref. 19. Part (b) displays the calculated spectra of the well, assuming indirect transitions and a doping spread of $\Delta z = 70$ Å. Lifetime broadening energy is 5 meV. The bound exciton peak labeled as A in the experimental spectra of part (a) is not shown in the calculated spectra of part (b).

This decrease is mainly due to nonradiative recombination processes that are more likely to occur at higher temperatures. The Q2D emission band would also diminish by two orders of magnitude if there were no other reasons for the decrease. Actually, the hole band decreases by more than four orders of magnitude in the temperature range under consideration. Thus, one is left with a net decrease of the experimental hole emission band by two orders of magnitude, compared with the half order of magnitude *increase* of the calculated band shown in Fig. 8. Such a strong decrease of the Q2D emission band with rising temperature has also been observed in a p-type δ-doping well in Si.[22] To explain this behavior at least qualitatively, the authors of Ref. 22 assumed a photoinduced minority carrier well introduced in Ref. 36 in a similar context. Such a well occurs if photoexcited holes are captured by the p-type δ-doping well; then the well is positively charged and attracts electrons. The electrons are confined close to the well, and the oscillator strengths of their transitions to confined hole states are strongly enhanced. If the temperature increases, the electrons are excited into unconfined states, which exhibit lower oscillator strengths; thus, the intensity of the Q2D emission band decreases.

To check this idea quantitatively, we have simulated the photoexcited holes by increasing the hole concentration of the well beyond that of the ionized acceptors. The charge neutrality of the sample assumed in our calculations creates the photoexcited electrons automatically. In Fig. 8(c), we depict the electrostatic potential profile for the p-type δ-doping structure shown in Fig. 8(a), i.e., with $N_s = 8 \times 10^{12}$ cm^{-2}, $\Delta z = 23.5$ Å, and $d = 2000$ Å, assuming a photoinduced carrier sheet density of $p_{\text{photo}} = 2 \times 10^{11}$ cm^{-2} (this value puts an upper limit[36]). The unnormalized PL spectra of the doping structure of Fig. 8(c) are depicted in Fig. 8(b) for the same temperatures as in Fig. 8(a). As expected, a temperature increase now leads to a strong decrease of the Q2D hole emission band. At a fixed temperature, the PL intensities are five times larger than in Fig. 8(a) without the photoinduced well.

Assuming the same photoinduced net charge sheet density as above, indirect PL spectra have been calculated also for the isolated p-type δ-doping well whose experimental PL spectra[19] are shown in Fig. 9(b). The parameters of the sample used in the calculations are $N_s = 3.9 \times 10^{12}$ cm^{-2}, $\Delta z = 75$ Å, and $d = 2000$ Å. If bound exciton peaks A are added to the calculated spectra of Fig. 9(b), they look quite similar to the experimental spectra of Fig. 9(a). This indicates that the photo-induced electron well in fact is responsible for the observed strong temperature decrease of the Q2D emission band in p-type δ-doping wells.

V. CONCLUSIONS

The above analysis has demonstrated that for a theoretical understanding of the experimental PL spectra from p-type δ-doping structures in GaAs the following findings are essential.

(i) Optical transitions between the confined hole and extended electron states of p-type δ-doping structures are rather indirect than direct in momentum spapce, due to the short range fluctuations of the impurity potential. Direct transitions result in PL spectra that are much richer of structures and much sharper than the PL spectra observed experimentally. Nevertheless, the calculated indirect spectra exhibit well-resolved peaks that compare well with the experimental ones. In many cases, a given PL peak cannot be attributed to one single occupied hole band but arises from two or more such bands.

(ii) The Q2D emission bands sensitively depend on the extended electron states. The latter are not only affected by the potential in the δ-doping region, as the hole states do, but also by the potential in the surrounding region. There, the potential depends on the sample structure as, for example, on the presence or absence of embedding electron barriers or, for the SL's under consideration, on the distance between neighboring δ-doping regions. Even if these regions are not seen by the confined holes, they may be essential for the extended electrons. For example, a SL of period 500 Å represents a series of isolated wells for holes, but it does not resemble the single barrier case for electrons. To achieve the latter, the period must be 2000 Å or larger.

(iii) If no electron confinement effects are included, theory predicts an increase of the Q2D emission band with rising temperature. In experiment, a strong decrease is observed. This discrepancy can be solved by assuming an electron confinement in photoinduced minority carrier wells. Then the Q2D band is enhanced considerably, provided the temperature is low and the electrons populate confined states. At higher temperatures, electrons are excited to less-well-localized states, and the Q2D band decreases.

The above findings suggest further experimental studies to be done on the PL spectra and other optical properties of p- and n-type δ-doping samples in GaAs. The observed enhancement of the Q2D emission band by a photoinduced minority carrier well could be even more important for n-type δ-doping samples than for p-type samples, as no Q2D electron emission band has been observed thus far. Using high excitation power, the optical enhancement effect could make this band observable. For comparison with theory, more precise experimental data on the hole level energies of

p-type δ-doping wells are highly desirable. Unfortunately, the indirect transitions that broaden the individual PL peaks carrying this information, are caused by the δ doping itself; one cannot expect sharper peaks from PL measurements by improving the sample quality, as this may be done in the case of heterostructure quantum wells. PL excitation and selectively excited P as well as photoreflectance could partially help to overcome this problem. One may also speculate as to whether infrared spectroscopy could be useful in this context. Infrared absorption measurements have been performed on p-type δ-doped Si samples[37–39] and n-type δ-doped GaAs samples[40] but, to our best knowledge, no infrared spectroscopy data are available for p-type δ-doped GaAs. Such measurements also could reveal whether p-type δ-doped GaAs samples are suitable for infrared detectors.

ACKNOWLEDGMENTS

The authors would like to thank CNPq, FAPESP, CAPES, and FINEP (Brazilian Funding Agencies) for partial financial support.

[1] K. Ploog, J. Cryst. Growth **81**, 304 (1987).
[2] E. F. Schubert, in *Epitaxial Microstructures*, edited by Arthur C. Gossard, Semiconductor and Semimetals (Academic, New York, 1994), Vol. 40, p. 1.
[3] A. Zrenner, F. Koch, and K. Ploog, Surf. Sci. **196**, 671 (1988).
[4] L. Ioriatti, Phys. Rev. B **41**, 8340 (1990).
[5] M. H. Degani, J. Appl. Phys. **70**, 4362 (1991).
[6] C. A. C. Mendonça, F. Plentz, J. B. B. Oliveira, E. A. Meneses, L. M. R. Scolfaro, D. Beliaev, S. M. Shibli, and J. R. Leite, Phys. Rev. B **48**, 12 316 (1993).
[7] S. M. Shibli, L. M. R. Scolfaro, J. R. Leite, C. A. C. Mendonça, F. Plentz, and E. A. Meneses, Appl. Phys. Lett. **60**, 2895 (1992).
[8] R. Enderlein, L. M. R. Scolfaro, J. M. V. Martins, and J. R. Leite, Superlattices Microstruct. **12**, 175 (1992).
[9] L. Chico, F. García-Moliner, and V. R. Velasco, Phys. Rev. B **48**, 11 427 (1993).
[10] L. M. R. Scolfaro, J. R. Leite, C. A. C. Mendonça, D. Beliaev, S. M. Shibli, E. C. F. da Silva, and E. A. Meneses, Mater. Sci. Forum **143-147**, 669 (1994).
[11] G.-Q. Hai, N. Studart, and F. M. Peeters, Phys. Rev. B **52**, 8363 (1995).
[12] D. Richards, J. Wagner, H. Schneider, G. Hendorfer, M. Maier, A. Fischer, and K. Ploog, Phys. Rev. B **47**, 9629 (1993).
[13] F. A. Reboredo and C. R. Proetto, Phys. Rev. B **47**, 4655 (1993).
[14] G. M. Sipahi, R. Enderlein, L. M. R. Scolfaro, and J. R. Leite, in *Proceedings of the 22nd International Conference on the Physics of Semiconductors*, edited by D. J. Lockwood (World Scientific, Singapore, 1995), p. 687.
[15] G. M. Sipahi, R. Enderlein, L. M. R. Scolfaro, and J. R. Leite, Phys. Rev. B **53**, 9930 (1996).
[16] G. M. Sipahi, R. Enderlein, L. M. R. Scolfaro, and J. R. Leite, in *Proceedings of the Seventh International Conference on Shallow-Level Centers in Semiconductors*, edited by C. A. J. Ammerlaan and B. Pajot (World Scientific, Singapore, 1997), p. 209.
[17] J. Wagner, A. Fischer, and K. Ploog, Phys. Rev. B **42**, 7280 (1990).
[18] J. Wagner, A. Ruiz, and K. Ploog, Phys. Rev. B **43**, 12 134 (1991).
[19] A. M. Gilinsky, K. S. Zhuravlev, D. I. Lubyshev, V. P. Migal, V. V. Preobrashenskii, and B. R. Semiagin, Superlattices Microstruct. **10**, 399 (1991).
[20] V. Ya. Aleshkin, A. V. Anshon, L. M. Batukova, E.V. Demidov, E. R. Demidova, B. N. Zvonkov, I. A. Karpovich, and I. G. Malkina, Fiz. Tekh. Poluprovodn. **26**, 1848 (1992) [Sov. Phys. Semicond. **26**, 1038 (1992)].
[21] M. El Allali, C. B. Sorensen, and E. Veje, J. Phys. IV **3**, 299 (1993).
[22] I. A. Buyanowa, W. M. Chen, A. Henry, W.-X. Ni, G. V. Hansson, and B. Monemar, Phys. Rev. B **53**, 9587 (1996).
[23] R. Enderlein, G. M. Sipahi, L. M. R. Scolfaro, J. R. Leite, and I. F. L. Diaz, Mater. Sci. Eng. B **35**, 396 (1995).
[24] E. O. Kane, in *Semiconductors and Semimetals*, edited by R. K. Willardson and A. C. Beer (Academic Press, New York, 1966), Vol. 1, p. 75.
[25] J. M. Luttinger and W. Kohn, Phys. Rev. **97**, 869 (1955).
[26] R. Enderlein and N. J. M. Horing, *Fundamentals of Semiconductor Physics and Devices* (World Scientific, Singapore, 1997).
[27] A. M. Cohen and G. E. Marques, Phys. Rev. B **41**, 10 608 (1990).
[28] R. Enderlein, G. M. Sipahi, L. M. R. Scolfaro, and J. R. Leite, Phys. Status Solidi B (to be published).
[29] L. Hedin and J. Lundqvist, J. Phys. C **4**, 2064 (1971).
[30] R. Enderlein (unpublished).
[31] D. Gershoni, C. H. Henry, and G. A. Baraff, IEEE J. Quantum Electron. **29**, 2433 (1993).
[32] Y. P. Varshini, Physica (Utrecht) **34**, 149 (1972).
[33] M. S. Skolnick, J. M. Rorison, K. J. Nash, D. J. Mowbray, P. R. Tapster, S. J. Bass, and A. D. Pitt, Phys. Rev. Lett. **58**, 2130 (1987).
[34] D. Olego and M. Cardona, Phys. Rev. B **22**, 886 (1980).
[35] Seong-II Kim, Moo-Sung Kim, Kyung Sook Eom, Suk-Ki Min, and Coochon Lee, J. Appl. Phys. **73**, 4703 (1993).
[36] V. M. Ansin, A. A. Rogachev, V. I. Stepanov, and A. B. Churilov, Pis'ma Zh. Eksp. Teor. Fiz. **45**, 436 (1987) [JETP Lett. **45**, 558 (1987)].
[37] G. Tempel, N. Schwarz, F. Müller, F. Koch, H. P. Zeindl, and I. Eisele, Thin Solid Films **182**, 171 (1990).
[38] J. S. Park, R. P. G. Karunasiki, Y. J. Mii, and K. L. Wang, Appl. Phys. Lett. **58**, 1083 (1991).
[39] G. Karunasiri, Jpn. J. Appl. Phys., Part 1 **33**, 2401 (1994).
[40] N. Schwarz, F. Müller, G. Tempel, F. Koch, and G. Weimann, Semicond. Sci. Technol. **4**, 571 (1989).